Biosensors and Bioelectronics 141 (2019) 111404

Contents lists available at ScienceDirect

Biosensors and Bioelectronics

journal homepage: www.elsevier.com/locate/bios

Enhancement of membrane protein reconstitution on 3D free-standing lipid bilayer array in a microfluidic channel

Won Bae Han[a], Dong-Hyun Kang[a], Jung-Hyun Na[b], Yeon Gyu Yu[b], Tae Song Kim[a,*]

[a] Center for BioMicrosystems, Korea Institute of Science and Technology, 5, Hwarang-ro 14-gil, Seongbuk-gu, Seoul, 02792, South Korea
[b] Department of Chemistry, Kookmin University, 77 Jeongneung-ro, Seongbuk-gu, Seoul, 02707, South Korea

ARTICLE INFO

Keywords:
Lipid
3-Dimensional lipid structure
Free-standing lipid bilayer
Protein reconstitution
Membrane protein

ABSTRACT

The bio-sensory organs of living creatures have evolved to have the best sensing performance. They have 3-dimensional protrusions that have large surface areas to accommodate a large number of membrane proteins such as ion channels and G-protein coupled receptors, resulting in high sensitivity and specificity to target molecules. From the perspective of mimicking this system, BLM, which has been used extensively as a platform for a single nanopore-based sensing systems, has some limitations, i.e., some residual solvent, low mechanical stability, small surface area for appropriate stability, and difficulty in high-throughput fabrication. Herein, to eliminate these limitations, a solvent-free, size-controllable, 3-dimensional free-standing lipid bilayer (3DFLB) structure array with high stability (~130 h) and high density (~300,000 cm^{-2}) is proposed, and its structural advantages for efficient and rapid protein reconstitution, compared to BLM, is demonstrated by human 5-HT_{3A} receptor assay as well as α-hemolysin assay. A continuous process of 3DFLB array fabrication, 5-HT_{3A} reconstitution, and 5-HT detections in a microfluidic channel proves the applicability of the proposed structures as a highly-sensitive sensing platform mimicking bio-sensory organs.

1. Introduction

Animals, including humans, have specific sensory organs that are highly developed in each species. For example, a dog senses odors that humans cannot perceive because their sense of smell is about 1000 times more sensitive(Czarnik, 1998). This is because of the difference in the degree of development of the olfactory cells that constitute the olfactory organ. Olfactory cells show the most efficient and precise performance as sensors by detecting specific target molecules with high selectivity and sensitivity by various membrane proteins, such as the ion channel in the membrane(Turner, 1997). Olfactory cells have evolved to have many cilia at their ends to enlarge the surface area, thereby accommodating a large number of membrane proteins, which maximizes their ability to efficiently and sensitively sense target molecules(DeMaria and Ngai, 2010). It is surprising that, to date, trained dogs still are used to detect drugs and explosives, indicating that portable bio/chemical sensors with the highest sensitivity and selectivity are bio-sensory organs that function by membrane proteins(Jezierski et al., 2014; Lazarowski and Dorman, 2014).

Over the last 30 years, significant attention has been focused on highly-sensitive biosensors that are capable of detecting a single molecule by mimicking cellular functions through the fabrication of artificial cell membrane structures(Cornell et al., 1997; Hirano-Iwata et al., 2010; Minami et al., 1991; Misawa et al., 2018; Rideau et al., 2018). Considering the role of the cell membrane, which completely separates the inside and outside of a cell, the bilayer lipid membrane (BLM) formed on an aperture or a microwell is an excellent candidate for sealing and facilitating the binding of relatively large membrane proteins, so it has been known to be one of the most suitable formats to mimic cell structure as a sensing platform. However, BLMs have relatively low mechanical stability, and attempts have been made to increase their mechanical stability by reducing the size of the aperture or the microwell or by changing its material and structure(Kalsi et al., 2014; Römer and Steinem, 2004; Urban et al., 2014). Although, such attempts extend the lifetime of BLMs to several tens of hours, reducing the size of the aperture or microwell causes the problem of reducing the surface area to which the membrane protein can be reconstituted.

Another important research topic in the development of sensors that mimic cell structure is the efficient reconstitution of membrane proteins into artificial cell membranes. In particular, human ion channel proteins are known to be more fragile than peptide pore protein(Tiefenauer and Demarche, 2012), and nAChR, GLuR, GaBaR, 5-HT_{3A}R, and hERGR have been reported to be successfully reconstituted to BLMs(Davis et al., 2007; Eray et al., 1994; Hirano-Iwata et al., 2016). As an attempt

* Corresponding author.
E-mail address: tskim@kist.re.kr (T.S. Kim).

https://doi.org/10.1016/j.bios.2019.111404
Received 4 January 2019; Received in revised form 24 May 2019; Accepted 1 June 2019
Available online 06 June 2019
0956-5663/

to reconstitute membrane proteins to BLMs, many methods have been proposed, such as inserting detergent-solubilized membrane proteins, making BLMs directly using proteoliposome (PL), fusing PL to BLMs, and inserting membrane proteins directly, but there is no universally applicable method(Syeda et al., 2008). Among the available methods, reconstituting membrane protein by fusing PL of several tens to a hundred nanometers in size has been used extensively to minimize the effects of detergent or organic solvent(Schindler and Rosenbusch, 1978) on the function and stability of the membrane protein(Bao et al., 2018; Eray et al., 1994; Hirano-Iwata et al., 2016; Studer et al., 2011). However, there is a need to improve the fusion efficiency of membrane proteins, and soluble NSF/alpha SNAP receptors (SNARE proteins), osmotic pressure, and centrifugal force have been used to increase the fusion efficiency of PL. But, the SNARE protein-assisted method is effective only for small-sized vesicles(Nordlund et al., 2014), and the centrifugal force-assisted method is difficult to use in a microfluidic device.

Herein, we describe our fabrication of a solvent-free 3D free-standing lipid bilayer (3DFLB) array, rather than a planar BLM, with a high density of 300,000 cm^{-2} in order to have a large surface area for easily reconstituting a large number of membrane proteins without affecting the stability of the membrane. The excellent sealing property and high stability (~130 h) of 3DFLB have been reported recently by our group(Kang et al., 2018). We numerically compared the reconstitution efficiency of α-hemolysin (αHL) to 3DFLB with BLM, and we found that 3DFLB can accommodate a large number of αHL, rather than BLM, by reacting directly and efficiently with the αHLs flowing in the microfluidic channel, which was attributed to its large surface area and structural advantages. We also successfully reconstituted human serotonin receptor (5-hydroxytryptamine receptor, 5-HT_{3A}) to 3DFLB using the PL fusion method, and we found that the reconstitution probability of 5-HT_{3A} was increased significantly in 3DFLB compared to BLM, resulting in high ion channel activity. The membrane protein 5-HT_{3A} is a neurotransmitter, ligand-gated ion channel associated with brain function(Maricq et al., 1991), which is one of the major types of channel proteins found with G protein-coupled receptors (GPCRs) in the central nervous system or sensory organs(Sato et al., 2008). We have reported the expression of high purity 5-HT_{3A} and the preparation of PL containing 5-HT_{3A}(Na et al., 2013), and, in this study, we used the oppositely-charged lipid-assisted fusion method to reconstitute 100-nm sized PL to 3DFLB effectively(Biner et al., 2016; Ishmukhametov et al., 2016; Lei and MacDonald, 2003). By forming a 3DFLB array that provided the stable reconstitution of membrane proteins, and analyzing the activity of 5-HT_{3A} by 5-hydroxytryptamine (5-HT) in the microfluidic device, we were able to confirm the efficiency of the selected reconstitution method on the 3DFLB array as well as the feasibility of utilizing the 3DFLB array as a highly-sensitive biosensing platform.

2. Materials and methods

2.1. Materials

The p-type (100) Si wafers we used were purchased from Hissan (Seoul, South Korea), and the AZ GXR-601 (46 cps) photoresist was purchased from Merck (Darmstadt, Germany). All phospholipids were purchased from Avanti Polar Lipids (Alabaster, AL, USA), i.e., 1,2-dioleoyl-sn-glycero-3-phosphocholine (DOPC); 1,2-Dioleoyl-sn-glycero-3-phosphoglycerol (DOPG); 1,2-dioleoyl-3-trimethylammonium-propane (chloride salt) (DOTAP); 1,2-dioleoyl-sn-glycero-3-phosphoethanolamine-N-(7-nitro-2-1,3-benzoxadiazol-4-yl) (ammonium salt) (NBD-PE); and 1,2-dioleoyl-sn-glycero-3-phosphoethanolamine-N-(lissamine rhodamine B sulfonyl) (Rhod-PE). Alexa fluor 488 dye (Succinimidyl Ester) and Fluo-4 (Pentapotassium Salt, cell impermeant) were purchased from Thermo Fisher Scientific (Waltham, MA, USA). The α-hemolysin (αHL) from Staphylococcus aureus; 5-Hydroxytryptamine hydrochloride (5-HT); Sucrose; 4-(2-hydroxyethyl)-1-piperazineethanesulfonic acid (HEPES); potassium chloride (KCl); calcium chloride ($CaCl_2$); ethylenediaminetetraacetic acid (disodium salt, dihydrate) (EDTA); Poloxamer 188; and all solvents were purchased from Sigma-Aldrich (St. Louis, MO, USA) and used as received. For bioassays, to prevent an unspecific adsorption of proteins, the microfluidic device was immersed in 3% Poloxamer 188 solution diluted in deionized water for 12 h and rinsed thoroughly with DI water.

2.2. Fabrication of the microfluidic device

The bottom PDMS channel (65 × 20 mm^2) with a 15 × 15 mm^2 slot for the insertion of the silicon chip was plasma bonded to a slide glass (75 × 25 mm^2). The top PDMS channel was made to have a fluidic channel (150 μm in height) for perfusing solutions, and it was fixed with a cover glass (30 × 25 mm^2) coated with 200-nm ITO (~50 Ω cm^{-1}). For performing all experiments, a lipid-coated silicon chip was inserted into the bottom PDMS channel, and the top PDMS channel was bonded on the bottom PDMS channel.

2.3. Fabrication of Si microwell arrays

Silicon wafers were cleaned with piranha solution (H_2SO_4: H_2O_2 = 3 : 1 (v/v)) for 15 min and rinsed thoroughly with DI water. Before spin-coating (500 rpm for 5 s and 3000 rpm for 30 s) the AZ GXR-601 photoresist on the Si wafer, a diluted HMDS (hexamethyldisiloxane) solution was spin-coated (500 rpm for 5 s and 3000 rpm for 30 s) to enhance the interaction of the photoresist with the surface of the wafer. After heating at 90 °C for 90 s to remove any remaining solvent, the wafer was irradiated by a UV lamp (20 mW/cm, 365 nm wavelength) through a mask for 4.2 s. The wafer was heated at 110 °C for 90 s and immersed in a developing solvent (MIF 300) for 35 s, followed by rinsing with DI water. Then, the wafer was baked at 110 °C for 60 s. Deep trench ion dry etching was conducted on the wafer, and the photoresist was removed with acetone in a bath sonicator and then in an oxygen plasma.

2.4. Selective coating of lipids into microwells

DOPC for the αHL assay, and DOPC + DOPG (molar ratio of DOPC: DOPG = 70 : 30) for 5-HT_{3A} ion channel assay were dissolved in chloroform, and the solvent was evaporated under a nitrogen atmosphere and then in vacuum. We added 0.5 mol% Rhod-PE For observation by fluorescent microscopy. An appropriate amount of trichloroethylene was added to a vial containing dried lipids to obtain the desired concentration. Si substrates with 15 × 15 mm^2 in which microwells are located in the center were cleaned in a piranha bath and rinsed with water. To increase the hydrophilicity of the surface, the substrates were treated with oxygen plasma (100 W, 500 mtorr, 90 s). The lipid solution was introduced on the substrate, and it was aspirated by a syringe pump at a rate of 30 mL/h after the substrate was spun at a rate of 100 rpm for 30 s. Then, it was dried in freeze dryer for more than 6 h to remove any traces of the solvent.

2.5. Formation of 3DFLB by electroforming method

Lipid-coated substrate was inserted in the microfluidic device shown in Fig. 1A. For size distribution and αHL assays, an AC electric field (0.33–5.33 V/mm, ramping step of 0.33 V/mm every 5 min) at a frequency of 10 Hz was applied between the indium tin oxide (ITO) electrode and the substrate while buffer A (100 mM sucrose) was flowing in the microfluidic channel at a flow rate of 20 μL/h. Initial hydration was performed at a rapid flow rate of 20 mL/h to minimize trapping air in the microfluidic channel and to remove air trapped in the microwells. For the 5-HT_{3A} ion channel assay, the microfluidic channel was filled with buffer B (0.5 mM HEPES, 0.5 mM KCl, 8 mM Sucrose, 45 μM EDTA, and 5 μM Fluo-4, pH 7.4), and the flow rate of

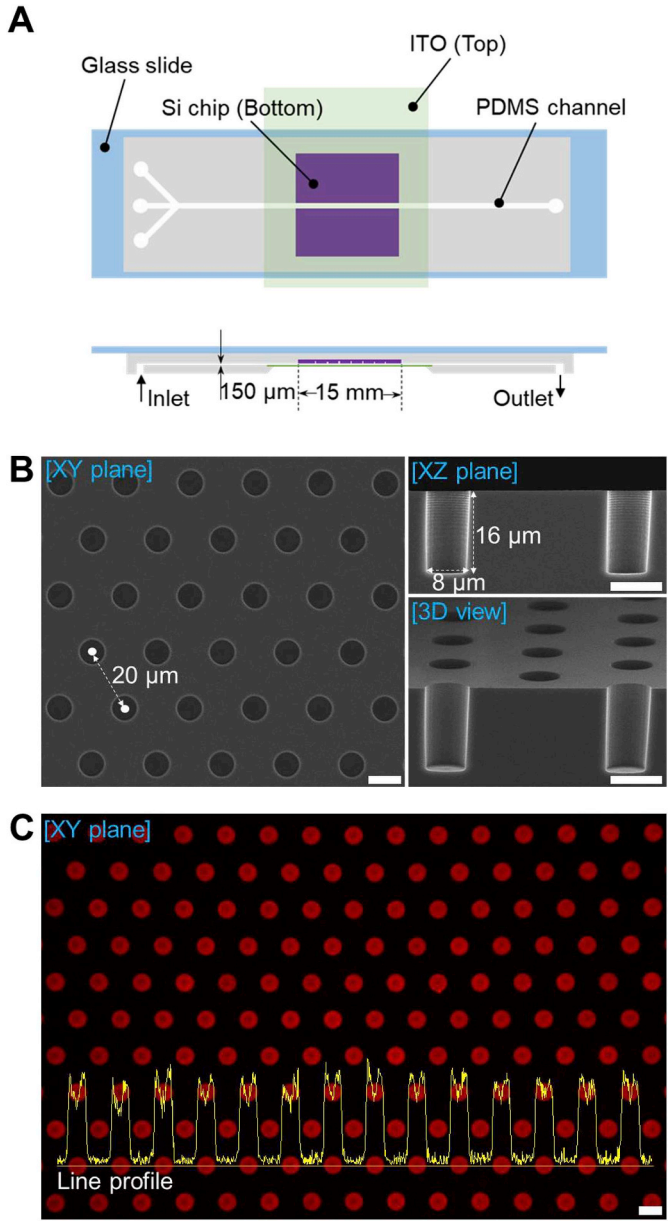

Fig. 1. Si microwell array for 3DFLB formation. (A) Schematic of the designed thin (150 μm in channel thickness) microfluidic channel for 3DFLB formation, solution exchanges, and bioassays. (B) Scanning electron microscopy images of microwell array (300,000 cm^{-2}) fabricated on Si substrate, where diameter, depth, and pitch were 8, 16, and 20 μm, respectively. (C) Fluorescent image of lipids (7 mM DOPC + 0.5 mol% Rhod-PE) selectively coated in a microwell array. Similar fluorescent intensities on microwells in the line profile indicate that the selective coating was performed with high uniformity. All scale bars are 10 μm.

the solution was 20 μL/h. At the same time, we applied an AC electric field with two steps, i.e., a growth step (1 kHz, 0.33–8.67 V/mm, ramping step of 0.33 V/mm every 5 min), and a sealing step (10 Hz, 5.33 V/mm for 10 min). Finally, the solution was exchanged with buffer C (0.5 mM HEPES, 0.5 mM KCl, and 8 mM sucrose, pH 7.4).

2.6. Formation of BLM by the water/oil/water method

The formation of BLM was performed based on the method proposed by Watanabe et al., (2014) with a small modification. First, the microfluidic device inserted with the microwell substrate was filled with buffer A for the αHL assay or with buffer B for the 5-HT_{3A} ion channel assay at a flow rate of 50 mL/h. Then, the solution was exchanged with 10 mg/mL of lipid solution (DOPC for αHL assay, or DOPC + DOPG (molar ratio of DOPC: DOPG = 70 : 30) for the 5-HT_{3A} ion channel assay) dissolved in hexadecane at a flow rate of 10 mL/h to form the first monolayer. The second monolayer was formed on the first monolayer by infusing the buffer solutions (buffer A for the αHL assay or buffer C for the 5-HT_{3A} ion channel assay) into the microfluidic channel at a flow rate of 1 mL/h. The efficiency for forming BLM was highly dependent on the flow rate of the solutions, and we achieved a BLM forming efficiency of ~15% using the conditions mentioned above.

2.7. Reconstitution of αHL on 3DFLB or BLM

To confirm the sealing of 3DFLB and BLM against molecules, buffer A with 5 μM Alexa fluor 488, was infused into the microfluidic channel. When the sealing was confirmed for 30 min, buffer A with 5 μM Alexa fluor 488 and αHL (0, 1, 5, and 10 μM) was infused at a flow rate of 20 μL/h for 150 min. And the change in the fluorescent intensity in 3DFLB or BLM was monitored by confocal microscopy with an acquisition frequency of 1 frame/min and an acquisition time of 1.54 s. The acquisition frequency and time were optimized to reduce the photobleaching effect and to monitor the continuous transporting behavior by αHL reconstitution.

2.8. Expression and purification of recombinant serotonin receptor (5-HT_{3A})

For the preparation of the 5-HT_{3A} expression vector, the cording genes of 5-HT_{3A} (amino acids 2–478; GenBank ID: CAA06442) were inserted downstream of the T7 promoter in the expression plasmid pRSETa vector (Thermo Fisher Scientific, USA). To express 5-HT_{3A} in a soluble form and purify the recombinant protein, the P9 protein from the *Psudomonas* phage phi6 (GenBank ID: ABB69810.1) and His6-tag also were inserted at the N-terminus and C-terminus cording genes of 5-$HT_{3A,}$ respectively(Na et al., 2013). The constructs were transformed into the *E. coli* strain Rossetta2 (DE3) (Merck-Millipore, Germany). The transformed cells were grown to OD_{600nm} of approximately 0.5 in TB medium at 37 °C that contained 50 mg/L of ampicillin. Expression was induced by 1 mM IPTG for 3 h at 37 °C. Recombinant proteins were purified using nickel-nitrilotriacetic acid agarose (QIAGEN, Germany).

2.9. Reconstitution of recombinant 5-HT_{3A} in liposomes

Reconstitution of P9-5-HT_{3A} was performed based on Na et al., (2013) with a small modification. Briefly, a mixture of DOPC, DOTAP, and NBD-PE lipids (molar ratio of DOPC: DOTAP: NBD-PE = 50 : 49.9: 0.1) was prepared in chloroform and dried under vacuum to make a lipid film. The lipid film was hydrated in buffer C for the 5-HT_{3A} ion channel assay or in buffer D (20 mM HEPES, 150 mM KCl, 7.5 μM $CaCl_2$, pH 7.2) for liposomal release assay at a concentration of 10 mg/mL, and we conducted 10 freezing-thawing cycles. Subsequently, the multilamellar liposome solution was extruded 19 times using Mini-Extruder (Avanti Polar Lipids, USA) through polycarbonate filters with pore sizes of 50 and 100 nm, respectively, to make unilamellar liposomes. The PLs were prepared by mixing the unilamellar liposomes with P9-5-HT_{3A} in buffer C or Buffer D containing 1% sarkosyl, at a 1:4000 protein-to-lipid molar ratio. After incubation at 4 °C for 3 h, the detergent in the mixture was removed by a PD MiniTrap G-25 desalting column (GE Healthcare, USA) after treatment with Bio-Beads (Bio-rad, USA) three times at 4 °C for a total of 3 h. Considering that the molar ratio of lipid to 5-HT_{3A} used in PL preparation was 4000:1, 100-nm sized PL contains approximately four 5-HT_{3A} pentamers.

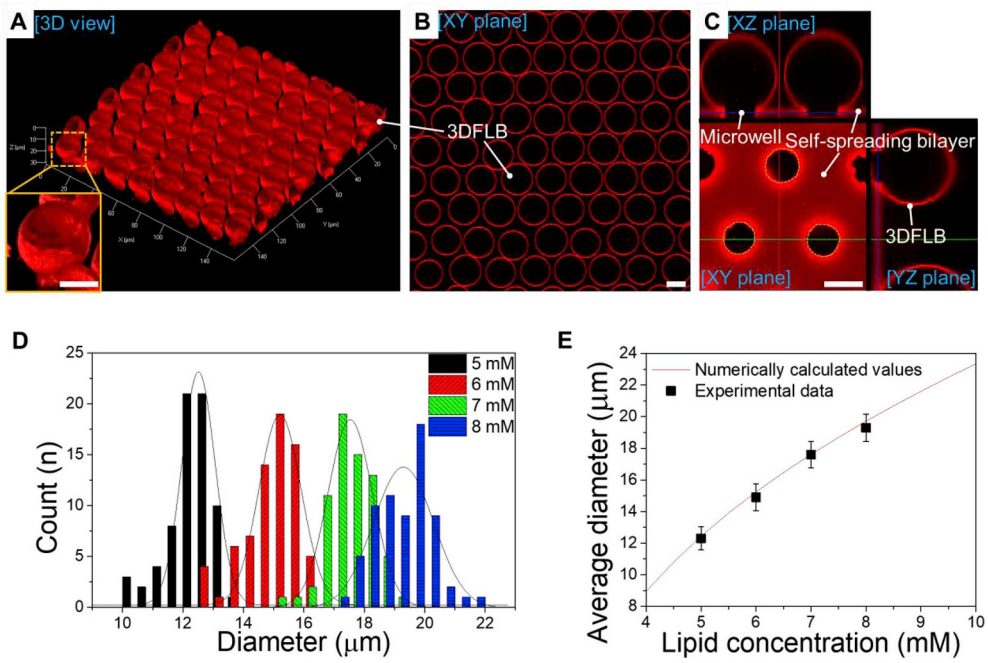

Fig. 2. Size-controllable 3DFLB array with high uniformity. (A) Confocal fluorescent 3D image of 3DFLB array formed on 7 mM DOPC (+0.5 mol% Rhod-PE)-coated microwell array by electroformation method. (B) The XY plane image of the 3DFLB array with high uniformity. The focus of the image was in the center of the 3DFLBs. (C) Orthogonal images of the 3DFLBs. All 3DFLBs were fixed to the microwell openings. And self-spreading lipid bilayer that was generated from lipids in microwells covered the entire surface of the Si substrate. The focus of the XY plane image was on the surface of the substrate. All scale bars are 10 μm. (D) Size-controllability of 3DFLB arrays by tuning lipid concentration from 5 to 8 mM. The size distribution curves of 3DFLBs were obtained from about 64 structures on each concentration (Fig. S3). The coefficient of variation (CV) values were low, i.e., ~5% as shown in Table S1, indicating that the high uniformity of the 3DFLB arrays. (E) The dependency of the size of 3DFLB array on the lipid concentration. As lipid concentration increased, the average diameter of 3DFLB increased, and this tendency was consistent with the numerical calculation (Fig. S4). In other words, the approach used in this experiment has great significance in that it can numerically predict the size of 3DFLB for various lipid concentrations, and that it can experimentally produce 3DFLB in the desired size.

2.10. Liposomal release assay

The channel opening activity of the reconstituted 5-HT_{3A} was measured using the Ca^{2+} ion release assay, as described previously(Na et al., 2013).

2.11. 5-HT_{3A} ion channel assay on 3DFLB or BLM

After 3DFLB and BLM were formed successfully, a 1% PL solution diluted in buffer C was infused through the microfluidic channel at a flow rate of 20 μL/h to deliver 5-HT_{3A} proteins in PL to the membranes of the 3DFLB or BLM. After the 30 min of the protein reconstitution step, the solution was exchanged with buffer C. In order to check the activity of the 5-HT_{3A} ion channel, buffer D (0.5 mM HEPES, 0.5 mM KCl, and 6.5 mM sucrose, pH 7.4) that contained 0.5 mM $CaCl_2$ and 30 μM 5-HT was infused, and, for the control experiments, buffer D that contained 5-HT or buffer D that contained $CaCl_2$ was infused. The amplification of the fluorescent intensity of Fluo-4 in 3DFLB and BLM was monitored with an acquisition frequency of 1 frame/min and an acquisition time of 1.54 s. The image of 'Difference' in Fig. 5C was obtained by using ImageJ software to subtract the image acquired at 0 min from the image acquired at 30 min.

2.12. Analysis of the reconstitution efficiency of αHL and 5-HT_{3A} on 3DFLB and BLM

We established a physicochemical model based on Fick's law to obtain the number of αHL pores reconstituted in each structure as follows.

$$\frac{dn}{dt} = -\mathrm{D}\cdot\mathrm{A}\cdot\left(\frac{dC}{dx}\right) \tag{1}$$

where n is the number of Alexa fluor 488 dye molecules that diffuse in the structure, D is the diffusion coefficient of Alexa fluor 488 ($D = \sim 4.6 \times 10^{-11}\ m^2 s^{-1}$ in buffer A),(Watanabe et al., 2014) A is the area of the αHL pore lumen, and C is the concentration difference of Alexa fluor 488 between the inside and outside of the structure. The diffusion coefficient of Alexa fluor 488 was corrected by considering the viscosity of buffer A ($\eta = 1.1$) by the Stokes-Einstein relation. From Equation (1), the passive transport of Alexa fluor 488 through αHL pores can be written as:

$$\mathrm{d}(V\cdot C(t)) = \left\{-D\cdot\left(\frac{d^2}{4}\cdot\pi\right)\cdot\left(\frac{C_0 - C(t)}{L}\right)\cdot dt\right\}\cdot N(t) \tag{2}$$

where N(t) is the number of αHL pores reconstituted on the structure, V is the volume of the structure ($V_{3DFLB} = 3.634 \times 10^{-15}\ m^3$ ($8.04 \times 10^{-16}\ m^3$ for BLM)), C_0 is initial concentration of Alexa fluor 488 on the background ($C_0 = 5$ μM), C(t) is the concentration of Alexa fluor 488 in the structure at given time, d is the diameter of the αHL pore ($d = \sim 1.5$ nm), and L is the length of the αHL pore ($L = \sim 10$ nm).

$$\mathrm{V}\cdot\frac{dC(t)}{dt} = -D\cdot\left(\frac{d^2}{4}\cdot\pi\right)\cdot\left(\frac{C_0 - C(t)}{L}\right)\cdot N(t) \tag{3}$$

If equation (3) were summarized for N(t):

$$\mathrm{N(t)} = \frac{4\cdot L\cdot V}{d^2\cdot\pi\cdot D}\cdot\frac{1}{C_0 - C(t)}\cdot\frac{dC(t)}{dt} \tag{4}$$

For the 5-HT_{3A} assay, it was assumed that calcium ions diffuse into 3DFLB through the 5-HT_{3A} ion channel activated by 5-HT based on Fick's law. The diffusion coefficient of calcium ions ($D = \sim 0.025 \times 10^{-9}\ m^2 s^{-1}$ in Buffer C,(Lynden-Bell and Rasaiah 1996) since the dynamic viscosity of 8 mM sucrose solution is nearly the same as that of DI water), the diameter of the 5-HT_{3A} ion channel (d = 0.76 nm)(Yang, 1990), and the length of the 5-HT_{3A} ion channel (L = 4 nm)(Thompson and R Lummis, 2006) were used.

2.13. Imaging and characterization

A Zeiss LSM 5 PASCAL axioplan 2 microscope (Carl Zeiss, Germany) was used to observe the lipid films deposited in microwells. The microscope was equipped with appropriate filter sets × 20 LD epiplan (numerical aperture 0.40) and × 50 LD epiplan (numerical aperture 0.50) objectives (ZEISS). The image was captured using a Retiga6000 CCD camera from Qimaging (Surrey, BC, Canada) and Micro-Manager software (version 1.4.17), and the image was analyzed with ImageJ

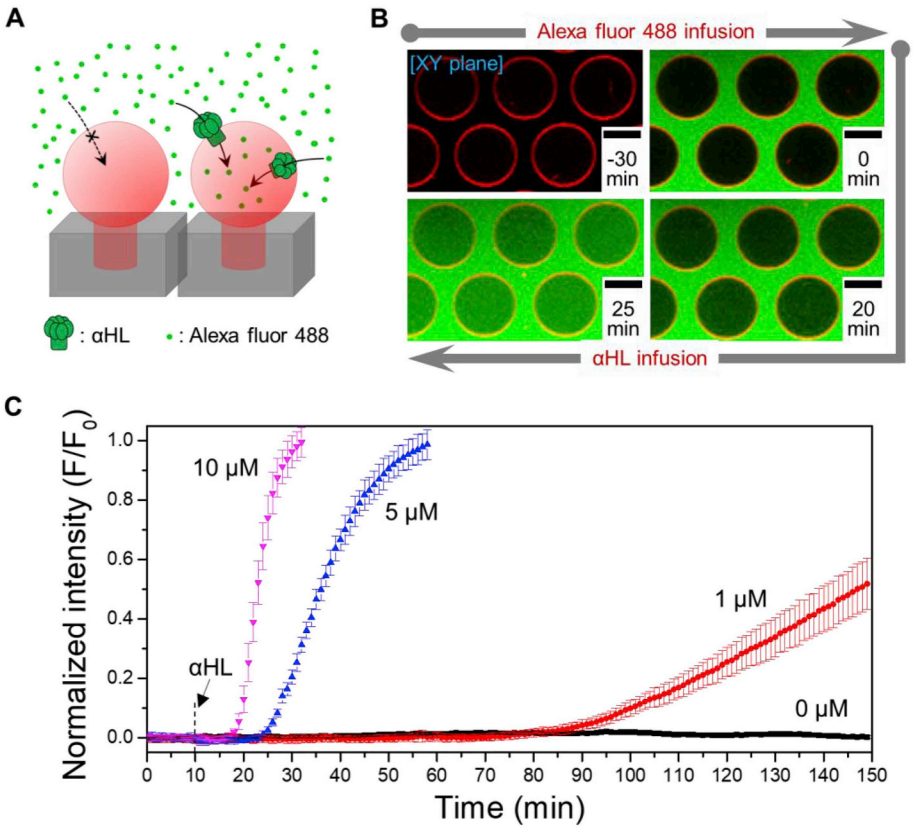

Fig. 3. Passive transport of dye molecules through αHL nanopores. (A) Schematic of the transport of Alexa 488 molecules (MW: 643.41) through αHL nanopores (~1.5 nm) on the 3DFLB array. The lipid membrane is impermeable to Alexa 488 molecules. (B) Confocal fluorescent time-lapse images of Alexa 488 diffusion into the 3DFLBs through αHL nanopores formed by 10 μM αHL infusion. −30 min: 3DFLBs were formed completely, and 5 μM Alexa 488 molecules were infused through the microfluidic channel. 0 min: αHL monomers started to reach the 3DFLB array. 20 min: αHL nanopores were formed on the membrane of the 3DFLBs, and Alexa 488 molecules were diffusing into the 3DFLBs through the αHL nanopores. 25 min: Alexa 488 molecules kept diffusing into the 3DFLBs, and the concentrations of Alexa 488 molecules inside and outside the 3DFLB became almost the same. All scale bars are 10 μm. (C) Normalized fluorescent intensity of Alexa 488 molecules inside the 3DFLBs over time (n = 15). As the αHL concentration increased from 0 to 10 μM, the transporting onset time and rate of Alexa 488 molecules became faster, indicating that the rate of pore formation was high at high αHL concentration. For the control experiment (αHL concentration = 0 μM), no change in the fluorescence was observed, indicating that 3DFLB maintained stability and sealing for more than 150 min.

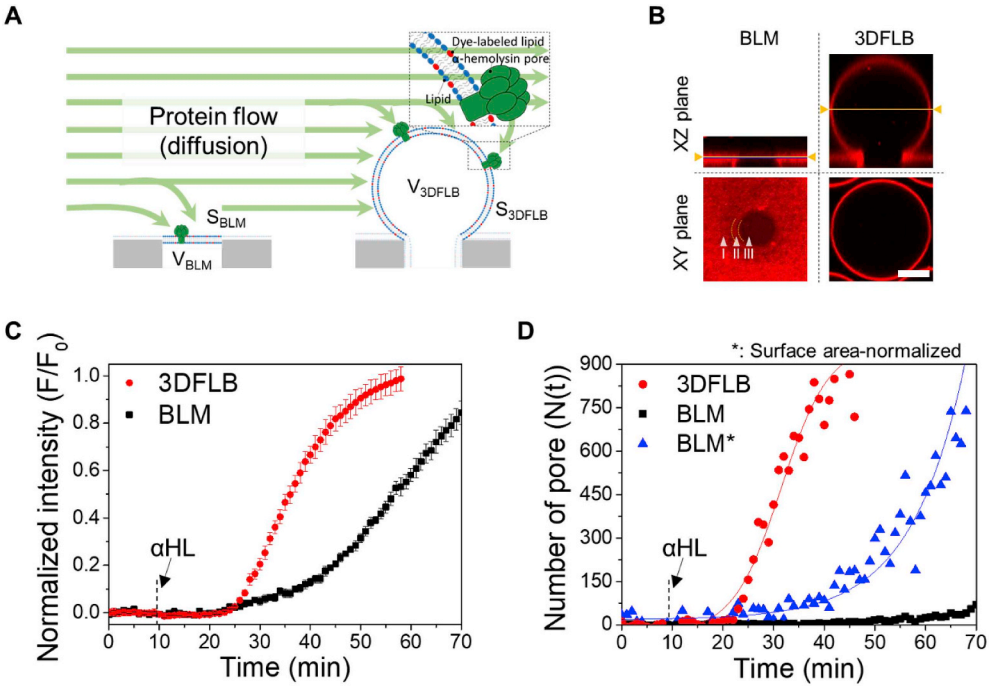

Fig. 4. Comparison of the reactivity of 3DFLB and BLM to proteins. (A) Schematic diagram illustrating the process by which proteins flow and bind to BLM and 3DFLB in the microfluidic channel. (B) Confocal fluorescent images of BLM and 3DFLB that formed on the Si microwell that had a diameter of 8 μm and a depth of 16 μm. The bottom image shows the XY plane of the yellow line in the top image. Region I, II, and the dark and round region III of the XY plane image of BLM represent the lipid monolayer-coated surface of the substrate, the Plateau-Gibbs border where a mixture of lipids and organic solvent was present, and the BLM surface where the lipid bilayer was formed, respectively. The scale bar is 5 μm. (C) Normalized fluorescent intensity of Alexa 488 molecules diffusing into BLM and 3DFLB upon 5 μM αHL infusion over time (n = 15). The onset times of Alexa 488 transportation in BLM and 3DFLB were similar, but the fluorescent intensity of 3DFLB increased more rapidly, suggesting that much more proteins were reconstituted on 3DFLB due to its surface area being larger than that of BLM. (D) Number of αHL nanopores reconstituted on BLM and 3DFLB, estimated from the plots in Fig. 4C by Equation (4). In order to compare the reactivity of 3DFLB with BLM irrespective of surface area effect, the number of αHL pores in surface area-normalized BLM were obtained by multiplying the number of αHL pores in BLM by the surface area difference between BLM and 3DFLB (18.4). Nevertheless, the number of αHL pores of the 3DFLB was much greater than that of the surface area-normalized BLM, meaning that the reactivity of the 3DFLB to αHL was enhanced by some factors other than the surface area effect. The factors would be the reduced BLM actual surface area by the Plateau-Gibbs boarder where protein reconstitution is impossible, the protruding shape of the 3DFLB, that reacts orthogonally and efficiently with the protein, and the protein depletion zone near the channel surface by the wall effect. (For interpretation of the references to color in this figure legend, the reader is referred to the Web version of this article.)

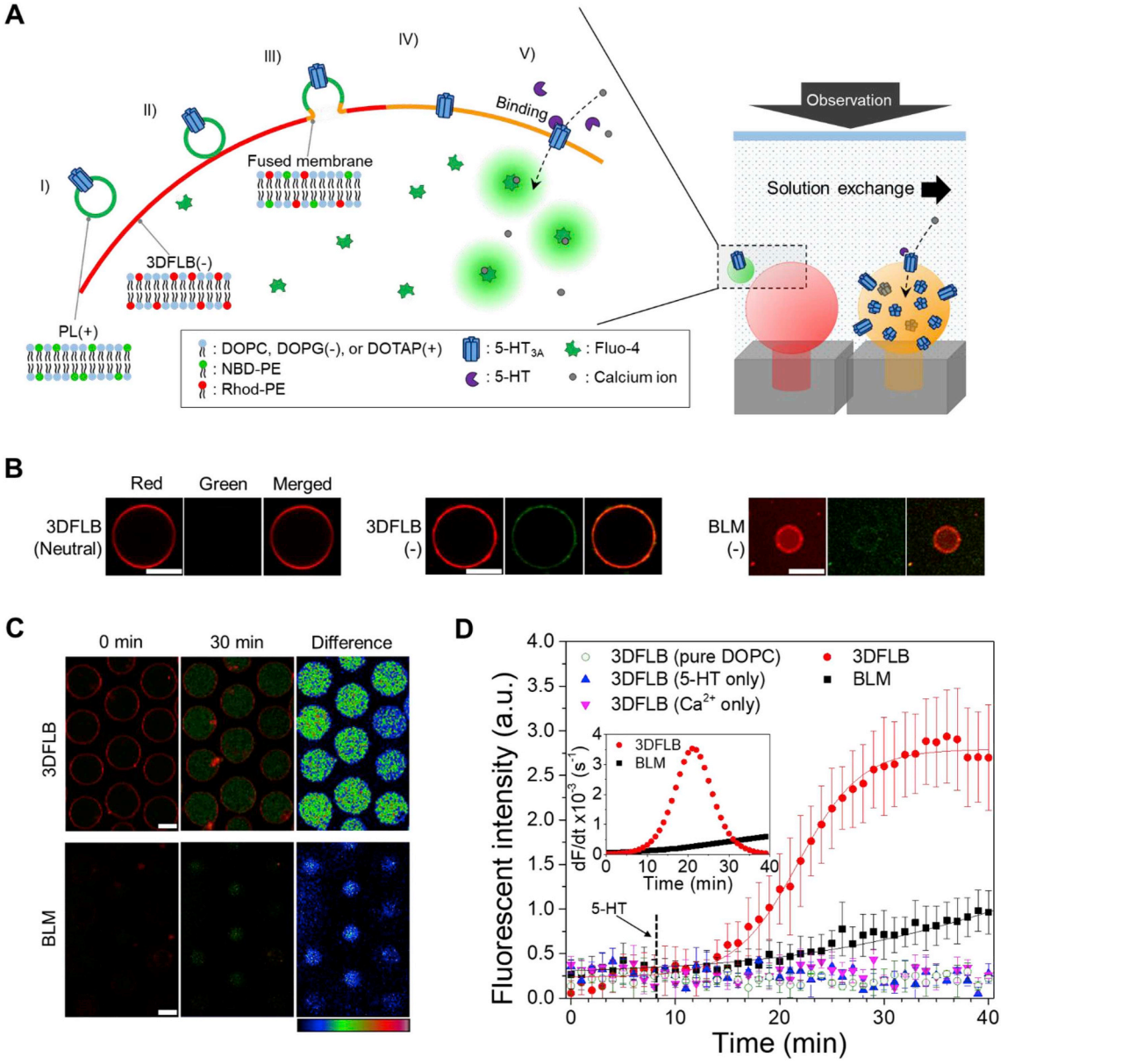

Fig. 5. Activation of human ion channels, 5-HT_{3A}, reconstituted on 3DFLB and BLM by ligand (5-HT). (A) Schematic diagram of the ligand-gated ion channel assay on 3DFLB. I) positively-charged PLs having 5-HT_{3A} receptors on their membrane are infused through the microfluidic channel. II) positively-charged PL binds to negatively-charged 3DFLB by electrostatic interaction between oppositely-charged lipids, DOTAP (+) and DOPG (−). III) oppositely-charged PL and 3DFLB are fused together, and their membranes start to merge into a continuous membrane. IV) fusion is completed, and 5-HT_{3A} receptor is transferred from the PL membrane to the 3DFLB membrane, preserving its orientation and activity. V) 5-HT activates the 5-HT_{3A} ion channel, so that calcium ions diffuse into 3DFLB, and the fluorescence of Fluo-4 is amplified by chelating calcium ions. (B) Reconstitution of 5-HT_{3A} receptors on 3DFLB and BLM by fusion of positively-charged (50% DOTAP) PL. Green fluorescence emitting from NBD-PE in PL did not appear on 3DFLB composed of pure DOPC, but it appeared on negatively charged (30% DOPG) 3DFLB and BLM, indicating that oppositely-charged lipids were a prerequisite for the fusion of PLs. (C) Fluorescent images of calcium ion diffusion into 3DFLB and BLM through 5-HT_{3A} ion channels activated by 30 μM 5-HT. For BLM, the fluorescence was measured 3 μm below the surface of BLM. The right image, Difference, shows the intensity difference between the left and middle images in the form of a color gradient. (D) Fluorescent intensity profiles inside 3DFLB and BLM upon 5-HT_{3A} activation by 5-HT over time (n = 12). The plots were fitted by the Boltzmann model (Adjacent R squared values for 3DFLB and BLM were 99.4% and 96.4%, respectively.). The fluorescence signal caused by the activation of 5-HT_{3A} was much higher than that of BLM, meaning that 3DFLB was more sensitive to 5-HT than BLM. The superimposed plot represents the increasing rate of fluorescent signals for 3DFLB and BLM. All scale bars are 10 μm.

software (version 1.50b). For the observation of lipid structures and the αHL and 5-HT_{3A} ion channel assays, we used an LSM 700 confocal microscope (Carl Zeiss, Germany) equipped with x 40 c-apochromat (numerical aperture 1.2). Images were acquired using ZEN software (blue edition) with a pinhole of 1 airy unit to obtain the best signal-to-noise ratio. Scanning electron microscopy (SEM, NOVA) measurements were conducted on the microstructured Si substrate to obtain the information of microwells' dimensions, i.e., diameter, depth, and pitch.

3. Results and discussion

3.1. Formation of 3DFLB on Si microwell arrays in a microfluidic channel

In order to produce bio/chemical sensors that mimick the 3D cellular structure that exists in bio-sensory organs, we fabricated the microfluidic device so that it could perform all of the desired processes, from the formation of the 3DFLB array to the sensing assays (Fig. 1A). A

microwell array with a population of 26,250 ($\sim 300{,}000\ cm^{-2}$) for the formation of 3DFLB was fabricated in the area of $3 \times 3\ mm^2$ of a $15 \times 15\ mm^2$ silicon chip. It was very uniform, and it had a deep depth of 16 μm, which facilitated the formation of regular 3DFLBs by promoting fusion through the confinement of the space in which the lipid structures grew. Also, it had an optimized pitch size of 20 μm that had a sufficiently high density (Fig. 1B). Selective coating of lipid (7 mM DOPC + 0.5 mol% Rhod-PE) into the microwell array was performed using trichloroethylene as a solvent that has the property of partially wetting the Si substrate (Fig. 1C, Fig. S2). Since trichloroethylene has a high vapor pressure of 69 mmHg (25 °C)(Gaube, 1985), it helps to form solvent-free lipid films through freeze-drying for 6 h, so the possibility of protein denaturation by the organic solvent(Korman et al., 2013) which is the main problem of conventional BLM-forming methods, was eliminated. The line profile superimposed in Fig. 1C shows that the fluorescent intensities of each well were nearly the same, indicating that selective coating with high uniformity was achieved properly.

A uniform 3DFLB array was fabricated by applying an AC electric field during rehydration (Fig. 2A and B). The fluorescence on the surface of the substrate around microwells represents a self-spreading bilayer(Furukawa et al., 2007) that propagated from the lipids deposited in the microwells (Fig. 2C). The 3DFLB that was produced resembled a giant unilamellar vesicle (GUV), but has a BLM-like, free-standing membrane that spans a microwell opening. Our group previously reported the details of dynamics in the microwells during the formation of 3DFLB using a transparent SU-8 microwell, which allowed us to see the inside of the microwell(Kang et al., 2018).

The size of the 3DFLB determines not only the size of the surface area but the number of absolute receptors that bind to the surface, which is directly related to the sensitivity of the biosensor(Uto et al., 1990). Therefore, it is very important to have the capability to control the size of the 3DFLB in designing an ion channel-based biosensor. In order to check the size controllability of the 3DFLB, we produced the 3DFLB from lipid films that were coated with various lipid concentrations, ranging from 5 to 8 mM. The size distribution curves obtained from the fluorescence images of the 3DFLBs (Fig. S3) were narrow and regular (Fig. 2D), indicating the high uniformity of the 3DFLBs, which had the low coefficient of variation values of 5 ± 1% as shown in Table S1. We assumed that this was attributable to the forming mechanism, in which the 3DFLB grew until the lipid film that was coated uniformly in the microwell was exhausted, meaning that the uniform coating of lipids is essential for the high uniformity of 3DFLB. As the lipid concentration increased, the average diameter of the 3DFLB increased (Fig. 2E), and this observation was consistent with the numerical calculation (Fig. S4), indicating that it can numerically predict the size of 3DFLB for various lipid concentrations and that it can experimentally produce 3DFLB of the desired size. This result supports possible applications that require a biocompatible, high-throughput container with a specific volume, such as a bioreactor as well as applications that require a certain surface area by controlling the size of the 3DFLB.

3.2. Comparison of passive transport activity of αHL on 3DFLB and BLM

When an artificial cell membrane structure is composed of a single lipid bilayer, it can reconstitute integral proteins, such as GPCRs and ligand-gated ion channels, and it can be used as a biosensing platform as well as a model membrane for studying the behavior of proteins. Therefore, it is important to confirm that the 3DFLB array consisted of a single lipid bilayer by using αHL, one of transmembrane proteins (Fig. 3A).

The 3DFLB array was infused sequentially with Alexa 488 (green fluorescence) and αHL in microfluidic channel (Fig. 3B). No changes in fluorescence were detected inside the 3DFLB array for 30 min from −30 min to 0 min, meaning that the 3DFLB maintained its seal against the external solute. Upon the infusion of αHL, the fluorescent intensity in the 3DFLB increased gradually for 25 min. These results indicated that the αHLs were bound to the 3DFLB membrane and formed pores that connected the inner and outer environments, which confirmed the unilamellarity and biofunctionality of the 3DFLB array.

The diffusion behavior of dye molecules was observed differently for various αHL concentrations (Fig. 3C). As the αHL concentration increased, the transport onset time of dye molecules became faster and the transport rate increased. This means that as the αHL concentration increased, the number of αHL monomers to be bound and the rate of pore formation increased. However, in the control experiment in which the αHL concentration was 0, the fluorescent intensity inside the 3DFLB was maintained for 150 min without any change. In addition, as previously reported by our group, the 3DFLB maintained stability over a period of about 130 h against a continuous mechanical perturbation of a mild flow and a few steps of solution exchange in the microfluidic device(Kang et al., 2018). The stability of conventional BLMs with surface area similar to 3DFLB and without supporting materials has been reported to be approximately 65 h(Hirano-Iwata et al., 2010; Oshima et al., 2013). We assumed that the reasons why 3DFLB has higher stability than BLM were that, unlike BLM, 3DFLB does not have any bilayer edges that are exposed directly to the aqueous solution, which can cause an unfavorable state and rearrangement(Bruce et al., 2002), and that 3DFLB also has structural elasticity like that of GUV. To the best of our knowledge, no artificial lipid membranes other than GUV array using a linker(Stamou et al., 2003) have been reported that maintained their sealing and stability for more than 100 h in the form of a 3D array structure fixed directly to the substrate.

One of the features of 3DFLB compared to BLM is its large surface area in unit space. A large surface area can accommodate a large number of proteins, thus improving the sensitivity of ion channel-based biosensing systems(Minami et al., 1991; Uto et al., 1990). Therefore, in order to demonstrate the high reactivity of 3DFLB with proteins due to its large surface area, αHL was introduced to both 3DFLB and BLM at the same conditions (Fig. 4A). The 3DFLB was formed from 7 mM lipid (average diameter of 17.6 μm), and BLM was formed in the same microwell, i.e., diameters of 8 μm and depths of 16 μm, using the water/oil/water method, as detailed in the experimental section (Fig. 4B, Fig. S5). The volume, surface area, and S/V ratios of the fabricated 3DFLB and BLM are presented in Table S2.

Upon the infusion of 5 μM αHL, the dye molecules diffused in 3DFLB and BLM through the αHL pores that formed, and the fluorescent intensity inside the structures increased (Fig. 4C). The onset time of the structures, i.e., when the fluorescent intensity began to increase, was about 20 min. However, the increasing rate of the fluorescent intensity was much faster in 3DFLB than in BLM. And, the fluorescent intensity in 3DFLB started to saturate at about 55 min, but BLM still showed a linear increase in the fluorescent intensity. These results indicated that, although the increase in the fluorescent intensity by the same amount of dye molecules was less in 3DFLB than in BLM because 3DFLB has a larger volume than BLM, many αHL pores were formed on the large surface area of 3DFLB, so rapid diffusion of the dye molecules occurred to offset the volume factor. To explain this, a physicochemical model was established by assuming that Alexa 488 diffuses through αHL pores based on Fick's law, and the number of αHL pores reconstituted in 3DFLB and BLM over time was obtained by Equation (4) (Fig. 4D, Fig. S6). The number of pores formed on BLM increased to about 80 upon the infusion of 5 μM αHL, and this value was believed to be reliable considering the results obtained by Wanatabe et al.(Watanabe et al., 2014), where 0, 1, or 2 pores were stochastically formed on BLM with diameters of 4 μm when 1 μg/mL (i.e., 0.033 μM) of αHL was infused. At about 35 min, the number of αHL pores in 3DFLB and the number in BLM were found to be different by a factor of more than 100, indicating that 3DFLB can accommodate proteins efficiently rather than BLM. To compare the behaviors of the two structures with the same surface areas, the number of αHL pores reconstituted on BLM was normalized by multiplying the surface area difference between the two structures as shown in Table S2. Here, it was assumed that the lipid structure with

the same surface area had the same αHL reconstitution probability. Although the number of αHL pores in the surface-normalized BLM theoretically should be similar to the number of αHL pores in 3DFLB, the difference was still a factor of about 10. This means that there were factors other than the surface area that affected the probability of αHL reconstitution. One such factor is the reduction of the actual surface area due to the Plateau-Gibbs border of BLM (Fig. S7). The Plateau-Gibbs border is an area in which there is a mixture of organic solvent and lipid, so protein reconstitution is impossible, and conventional BLM-forming methods produce the Plateau-Gibbs border. Since the BLM formed in this study has a Plateau-Gibbs border in a ring shape on the outer part of the microwell, the biofunctional surface area of the BLM was reduced. The actual diameter and surface area decreased from 8 μm and 50.3 μm^2 to 6.5 ± 0.45 μm and 33.3 ± 4.5 μm^2, respectively. The 34% reduction of the actual surface area caused a decrease in the number of αHL pores in BLM. Even considering the reduced actual surface area, 3DFLB had an αHL pore number that was 6–7 times greater than BLM. On the other hand, a BLM-forming method using vesicle rupture(Sumitomo et al., 2012) does not produce the Plateau-Gibbs border, but it is not suitable as an effective sensing platform because it is difficult to form a high-density lipid structure in the desired region. A second factor is that, unlike BLM, there is the structural effect of 3DFLB protruding from the substrate into the microfluidic channel. Although the extent of the effect was difficult to measure quantitatively, the protruding architecture of 3DFLB increased the probability of direct and orthogonal contact with the αHL proteins flowing in the microfluidic channel. BLM could hardly meet orthogonally with the proteins, but half of the surface area of 3DFLB could meet orthogonally with the proteins. Therefore, the increased probability of 3DFLB coming in contact with the proteins led to an increase in the number of αHL pores in 3DFLB. A third factor is the concentration gradient of protein flowing through the microfluidic channel. There is a very low concentration of molecules flowing in the microfluidic channel (depletion zone) at the surface of the channel due to the wall effect in laminar flow(Doyeux et al., 2011; Kanjirakat and Sadr, 2016). Therefore, the BLM that was collinear with the surface of the channel had the probability of encountering the low concentration of protein. This caused a decrease in the number of αHL pores in BLM. Based on these results, it is expected that 3DFLB can accommodate many proteins faster and more efficiently than BLM, and it also has a better probability of detecting target molecules.

3.3. Enhanced reconstitution efficiency and activity of human 5-HT_{3A} ion channel on 3DFLB

The reconstitution of a large number of membrane proteins on an artificial cell membrane is one of the key technologies for ion channel-based sensors, including the 3DFLB sensing platform that mimicks biosensory organs, and, especially, the low reconstitution efficiency of proteins must be improved. Therefore, to study the effect of the large surface area and structural advantages of 3DFLB on the biofunctional behavior of accepting ion channel receptors and detecting a specific ligand, we reconstituted 5-HT_{3A} to 3DFLB and BLM, and compared the ion channel activities of the two structures activated by 5-HT in the microfluidic channel (Fig. 5A).

Oppositely-charged lipid-assisted fusion of PL to reconstitute membrane proteins in lipid structures depends strongly on the charged lipid concentration of the membranes and the ionic strength of the external medium (buffer), and these factors determine the status of fusion, such as only binding, hemifusion, or complete fusion(Pantazatos et al., 2003; Stebelska et al., 2005). And, as the concentration of the charged lipid in the membrane increased, it became more difficult to form a uniform 3DFLB array by electroformation(Rodriguez et al., 2005). Therefore, the maximum DOPG (30%) that can attain a forming efficiency of 90% or more of 3DFLB under the ionic strength of buffer B was added to 3DFLB, and 50% DOTAP that can keep the PL membrane stable while maximizing the attractive electrostatic force between 3DFLB and PL was added to PL. Also, optimizing the size of PL is very important, because the activity of the protein is influenced greatly by the size of PL when an expressed and purified protein is reconstituted into PL. When the diameter was less than 50 nm, the probability of protein activation was 20% (activity: 1 success in 5 attempts) and the stability of the protein was very poor (Fig. S8). It was assumed that if 5-HT_{3A} with a diameter of 5 nm and a height of 10 nm(Thompson and R Lummis, 2006) were located in a small liposome with a large curvature, the intrinsic conformation and orientation of the protein would deteriorate. In addition, the stability of liposome decreases as the size decreases(Lin et al., 2012). And the fusion of vesicles is highly dependent on size(Biner et al., 2016). If a PL that is too large is used, the membrane's positive curvature is decreased, and the fusion rate and probability decrease(Biner et al., 2016; Kozlov and Chernomordik, 2015). This is because, if the membrane's positive curvature is small, the tension of the membrane that drives the formation and expansion of the fusion pore for the complete fusion after the contact of vesicles by electrostatic interaction decreases. Therefore, to efficiently reconstitute proteins, we optimized the size of PL to 100 nm (activity: 5 successes in 5 attempts), keeping the protein activity stable and the fusion probability high.

To check the dependence of fusion on the charged lipid concentration, 3DFLB composed of 100% DOPC (left), 3DFLB that contains 30% DOPG (center), and BLM that contains 30% DOPG (right) were fused with 100-nm sized PL containing 50% DOTAP in buffer C (Fig. 5B). In the 3DFLB composed of 100% DOPC without charged lipids, the green fluorescence emitted from NBD-PE on PL did not appear on the membrane, indicating that the electrostatic interaction of 3DFLB with PL was too weak to fuse the membranes, even though 0.5 mol% of negatively-charged, Rhod-PE for fluorescence imaging was added in 3DFLB. However, for 3DFLB that contained 30% DOPG, fusion with PL occurred, and green fluorescence was observed on the 3DFLB membrane. To investigate the fusion by electrostatic interaction more closely, after PL infusion, we observed a change in the green fluorescence on the 3DFLB membrane over time (Fig. S9). Green fluorescence began to appear at about 9 min after the infused PLs reached the 3DFLB in the microfluidic channel, and then the fusion of many PLs occurred within about 15 min. Interestingly, small particles that emitted intense fluorescence appeared on the 3DFLB membrane, and these particles were retained over time, but some disappeared. We assumed that these were PL aggregates or invaginations produced by the fusion of many PLs(Lei and MacDonald, 2003). From these optical results, it was impossible to confirm whether PL is simply bound, hemifused, or completely fused to 3DFLB due to the limitation of the resolution of the confocal microscope. However, since the green fluorescence was present continuously (partially discrete) on the 3DFLB membrane, it was estimated that sufficient numbers of PLs were fused completely to 3DFLB, resulting in a mixture of 3DFLB and PL membranes. Even in the case of BLM, very light green fluorescence was observed on the surface, indicating that the fusion of PLs occurred. Both green fluorescence and red fluorescence were observed on the surface of the substrate because unspecific fusion of PLs occurred on the self-spreading lipid bilayer on the surface.

As 5-HT and calcium ions were infused simultaneously into 3DFLB and BLM in which 5-HT_{3A} had been reconstituted successfully, the 5-HT_{3A} ion channels became activated, resulting in the amplification of the fluorescence inside the structures (Fig. 5C). When 5-HT binds to the binding sites of 5-HT_{3A}, the cations ionized in the buffer diffused through the ion channel while keeping the osmolarity in 3DFLB and BLM at the same level, and the fluorescent intensity of Fluo-4 was amplified by chelating the calcium ions. Changes in the fluorescent intensity inside 3DFLB and BLM before and after infusion of 5-HT were evident, indicating that 5-HT_{3A} ion channels were activated successfully by 5-HT. Interestingly, amplification of the fluorescent intensity was much greater in the case of 3DFLB than BLM under the same conditions.

In order to analyze the activation of 5-HT_{3A} in detail, we observed

the changes in fluorescence inside the structures over time after the infusion of 5-HT (Fig. 5D). Upon the infusion of 5-HT through the microfluidic channel, the ion channels began to activate after about 8 min for 3DFLB and after 10 min for BLM. As the solution exchange proceeded completely, the concentration of 5-HT increased up to 5 μM, and the rate of amplification of the fluorescence increased. At 30 min, the fluorescent intensity for 3DFLB became saturated, but the fluorescent intensity for BLM was still increasing. Here, it is noting that the Fluo-4 (dissociation constant for Ca^{2+} at 22 °C: 345 nM)(Gee et al., 2000) present inside 3DFLB has two chelating agents and has a high affinity for calcium ions, so, when only 10 μM calcium ions were diffused into 3DFLB, the fluorescence of all of the 5 μM Fluo-4 was amplified by chelating the calcium ions. Therefore, even if the calcium ions continued to diffuse into 3DFLB while keeping the osmolarity and electrochemical gradient in equilibrium, there are no further changes in the saturated fluorescent intensity inside 3DFLB, except for the photobleaching effect. The peak of the increasing rate of fluorescent intensity (dF/dt) of 3DFLB was higher than that of BLM, and also the peak arrival time of 3DFLB was much shorter than that of BLM. We concluded that the high dF/dt and the short peak arrival time were attributable to the high population of 5-HT_{3A} and the efficient and rapid binding of 5-HT, respectively. We reached this conclusion because the transport rate of calcium ions increases as the number of reconstituted protein increases, resulting in an increase in dF/dt, and the efficient and rapid binding of the agonist to protein increases the probability and rate of activation of the reconstituted proteins, resulting in a faster activation onset time and a shorter peak arrival time. It is noting that Fluo-4 could not escape out of 3DFLB, and calcium ions could not enter 3DFLB without ion channel activation. This was confirmed by the result of the control experiment in which the fluorescence inside 3DFLB was maintained for 40 min when infused with either 5-HT or calcium ions. Also, even though 5-HT and calcium ions were infused simultaneously into 3DFLB consisting of pure DOPC, the fluorescence inside 3DFLB did not change, reconfirming that there was no protein reconstitution on 3DFLB due to no fusion of PL to 3DFLB, as confirmed in Fig. 5B.

In order to quantitatively analyze the efficiency of protein reconstitution by the fusion of PL to 3DFLB and also the high reactivity of 3DFLB to 5-HT, we calculated the number of ion channels that were activated gradually by the 5-HT by the physicochemical model established to obtain the number of αHL pores, as detailed in the experimental section. The numbers of ion channels activated in 3DFLB, BLM, and surface area-normalized BLM were 18, 0.4, and 7, respectively, at 20 min when the dF/dt of 3DFLB was the highest (Fig. 6A). This means that, in 3DFLB, 18 ion channels were kept open and transported calcium ions passively and continuously like αHL pore. As in the case of the αHL assay, the number of ion channels opened per second in 3DFLB

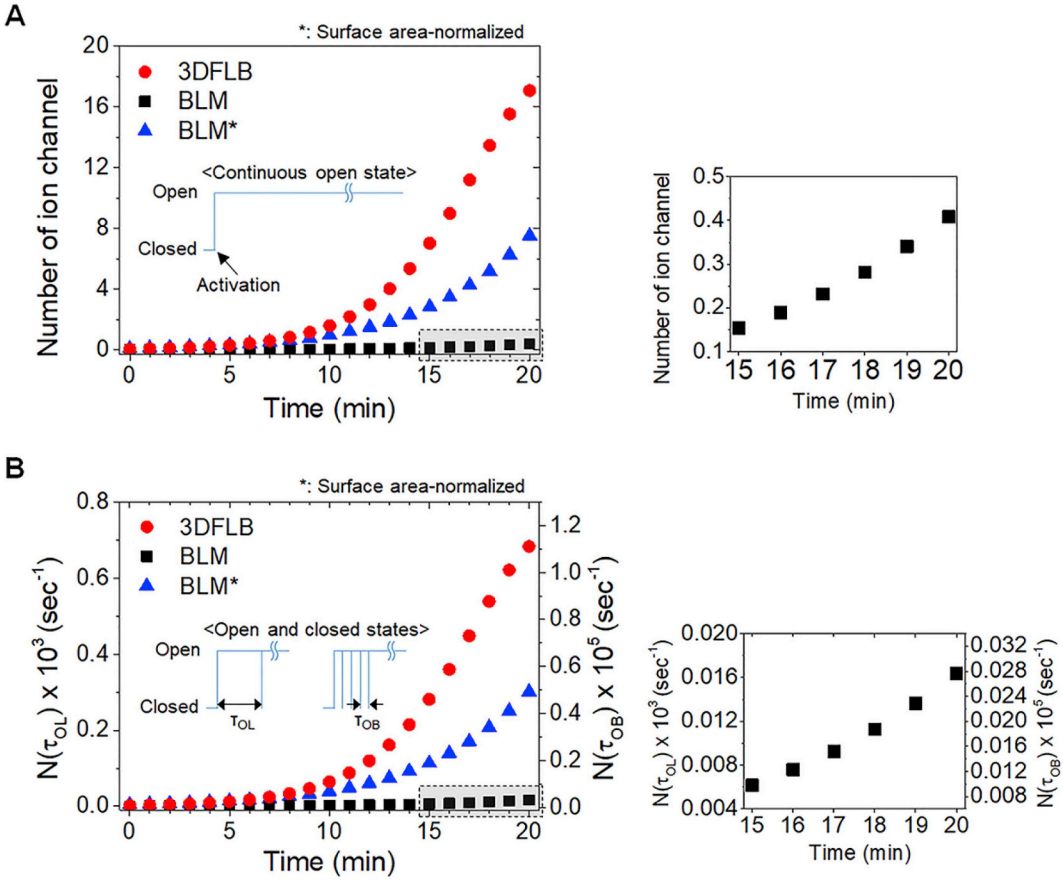

Fig. 6. Comparison of the number of 5-HT_{3A} ion channels activated on 3DFLB and BLM. (A) Number of ion channels calculated from the fluorescent intensity profiles of Fig. 5D by Equation (4). It postulates that once an ion channel was activated, it would not be deactivated or desensitized, so that the diffusion of calcium ions through it occurred passively and continuously. The inset schematic shows the status of an ion channel upon activation. The enlarged graph (right) shows the highlighted box area. (B) Number of activated ion channels having long or brief opening times. In fact, when an ion channel is activated by an agonist, it has either open or closed states with an opening time dependent on the surrounding environment, such as the concentration of the agonist. Therefore, considering long (τ_{OL}: 25 ms) or brief (τ_{OL}: 0.15 ms) opening times of the 5-HT_{3A} single ion channel for the 5-HT concentration of 30 μM, we calculated the number of activated ion channels from Fig. 6A. At 20 min, where the increase rate of fluorescence signal was the highest, there was an open activity of the ion channel from 700 to 110,000 times per second in 3DFLB. The number of ion channel openings in 3DFLB was about 40 times higher than that of BLM and even more than twice that of the surface area-normalized BLM. The inset schematic shows the status of an ion channel that had a long (τ_{OL}) or a brief (τ_{OL}) opening times. The enlarged graph (right) shows the highlighted box area.

was higher than in BLM and in the surface-normalized BLM, so the advantages of 3DFLB were still valid in the 5-HT_{3A} assay. However, the protein-binding efficiency of 3DFLB was more than 100 times higher than that of BLM in the αHL assay, but the difference of protein binding efficiency between 3DFLB and BLM was only about 40-fold in the 5-HT_{3A} assay. We concluded that the reason for this was that an extra amount of channel proteins might be bound to BLM since it was reported earlier that the hydrocarbon solvent of the Plateau-Gibbs border region present in BLM promotes the fusion of PL(Cohen, 1984; Gutsmann et al., 2015; Hirano-Iwata et al., 2016). On the other hand, when an ion channel is activated by an agonist, it has either open or closed states, with the opening time depending on the surrounding environment, such as the concentration of the agonist. The opening time of the 5-HT_{3A} single ion channel for the 5-HT concentration of 30 μM used in this study is known to be approximately 25 ms for the longest open time (τ_{OL}) and 0.15 ms for the brief open time (τ_{OB}) (Corradi et al., 2009). Therefore, the number of ion channels opened per second can be obtained from Fig. 6A by introducing τ_{OL} and τ_{OB} (Fig. 6B). As a result, the opening activity of the ion channel was at least 700 times per second and a maximum of 110,000 times per second in 3DFLB. The number of ion channel openings of 3DFLB was approximately 40 times higher than that of BLM, and it was even more than twice as many as that of the surface area-normalized BLM. This means that the PL fusion method using oppositely-charged lipids was able to efficiently reconstitute a larger number of proteins in 3DFLB than in BLM. In other words, 3DFLB has an improved protein reconstitution efficiency, which was attributed to its large surface area and structural advantages. Thus, it will be an alternative to conventional lipid structures including BLM, as a highly-sensitive sensing platform.

4. Conclusion

Over the last 30 years, much attention has been paid to the fabrication and application of single or multiple BLM structures spanning a small aperture or microwell array(Heitz et al., 2009; Korman et al., 2013; Oshima et al., 2013; Ota et al., 2011; Römer and Steinem, 2004; Sumitomo et al., 2012; Urban et al., 2014; Watanabe et al. 2014, 2016). The application of ion channel as a biosensor is one of the main research objectives, but progress in the development of a sensing system using an artificial cell membrane and membrane protein as the receptor has been delayed due to 1) the low stability of the BLM structure, 2) the low reconstitution efficiency of membrane protein, 3) difficulty in making high-density artificial cell membrane structures that are free of organic solvents, and 4) the lack of on-chip technology that would enable continuous batch execution of the formation of artificial cell membrane structures, reconstitution of membrane proteins, and bioassays. In this study, we fabricated a solvent-free 3DFLB array with the desired composition and size, supplied a PL that contained membrane proteins, and performed a bioassay sequentially in the designed microfluidic device. The 3DFLB array had the advantages of high stability (~130 h), large surface area (equivalent to the surface area of BLM with a diameter of ~45 μm), and a high population (~300,000 cm^{-2}). The protruding architecture of 3DFLB was similar to the cell structure found in bio-sensory organs, such as the cilia in the nose and the microvilli in the tongue, and, when compared to previously reported GUV arrays with linkers(Stamou et al., 2003), the 3DFLB array was superior in terms of ease of fabrication and ease of application to biosensing systems.

Having successfully performed the bioassays in the microfluidic device, we propose the possibility of applying this system as a sensing platform using the 3D artificial cell membrane structure and membrane proteins. In particular, due to the enhanced protein reconstitution efficiency that is attributed to the structural advantages of 3DFLB, a large number of membrane proteins that are essential for an ion channel-based sensing system could be reconstituted to the fabricated 3DFLB. Therefore, we expect that, in the near future, 3DFLB reconstituted with various membrane proteins with high density will be useful in various fields that require high selectivity and sensitivity, such as artificial sensory organs, medical care, environmental monitoring, and safety screening.

CRediT authorship contribution statement

Won Bae Han: Conceptualization, Methodology, Formal analysis, Investigation, Writing - original draft. **Dong-Hyun Kang:** Formal analysis, Investigation. **Jung-Hyun Na:** Formal analysis, Investigation. **Yeon Gyu Yu:** Formal analysis, Investigation, Supervision. **Tae Song Kim:** Conceptualization, Writing - review & editing, Supervision.

Acknowledgements

This research was supported by KIST Institutional Program (2E29200). We are also indebted to Dr. Young Jun Kim and Dr. Kuiwon Choi, Director, Korea Institute of Science and Technology Europe, Germany for the α-hemolysin experiments.

Appendix A. Supplementary data

Supplementary data to this article can be found online at https://doi.org/10.1016/j.bios.2019.111404.

References

Bao, H., Das, D., Courtney, N.A., Jiang, Y., Briguglio, J.S., Lou, X., Roston, D., Cui, Q., Chanda, B., Chapman, E.R., 2018. Dynamics and number of trans-SNARE complexes determine nascent fusion pore properties. Nature 554 (7691), 260–263.
Biner, O., Schick, T., Muller, Y., von Ballmoos, C., 2016. Delivery of membrane proteins into small and giant unilamellar vesicles by charge-mediated fusion. FEBS Lett. 590 (14), 2051–2062.
Bruce, A., Alexander, J., Julian, L., Martin, R., Keith, R., Peter, W., 2002. Molecular Biology of the Cell, fourth ed. Garland Science, New York.
Cohen, F.S., 1984. Parameters affecting the fusion of unilamellar phospholipid vesicles with planar bilayer membranes. J. Cell Biol. 98 (3), 1054–1062.
Cornell, B.A., Braach-Maksvytis, V.L.B., King, L.G., Osman, P.D.J., Raguse, B., Wieczorek, L., Pace, R.J., 1997. A biosensor that uses ion-channel switches. Nature 387, 580.
Corradi, J., Gumilar, F., Bouzat, C., 2009. Single-channel kinetic analysis for activation and desensitization of homomeric 5-HT(3)A receptors. Biophys. J. 97 (5), 1335–1345.
Czarnik, A.W., 1998. A sense for landmines. Nature 394, 417.
Davis, R.W., Flores, A., Barrick, T.A., Cox, J.M., Brozik, S.M., Lopez, G.P., Brozik, J.A., 2007. Nanoporous microbead supported bilayers: stability, physical characterization, and incorporation of functional transmembrane proteins. Langmuir 23 (7), 3864–3872.
DeMaria, S., Ngai, J., 2010. The cell biology of smell. J. Cell Biol. 191 (3), 443–452.
Doyeux, V., Podgorski, T., Peponas, S., Ismail, M., Coupier, G., 2011. Spheres in the vicinity of a bifurcation: elucidating the Zweifach–Fung effect. J. Fluid Mech. 674, 359–388.
Eray, M., Dogan, N.S., Liu, L., Koch, A.R., Moffett, D., Silber, M., Van Wie, B.J., 1994. Highly stable bilayer lipid membranes (BLMs) formed on microfabricated polyimide apertures. Biosens. Bioelectron. 9 (4–5), 343–351.
Furukawa, K., Sumitomo, K., Nakashima, H., Kashimura, Y., Torimitsu, K., 2007. Supported lipid bilayer self-spreading on a nanostructured silicon surface. Langmuir 23 (2), 367–371.
Gaube, J., 1985. T. Boublík, V. Fried, E. Hála: the Vapour Pressures of Pure substances-Selected Values of the Temperature Dependence of the Vapour Pressures of Some Pure Substances in the Normal and Low Pressure Region, vol. 17 Physical Sciences Data, Elsevier Science Publishers, Amsterdam, Oxford, New York, Tokyo 1984. 972 Seiten, Preis: Dfl. 450,—. Berichte der Bunsengesellschaft für physikalische Chemie 89(3), 352-352.
Gee, K.R., Brown, K.A., Chen, W.N., Bishop-Stewart, J., Gray, D., Johnson, I., 2000. Chemical and physiological characterization of fluo-4 Ca(2+)-indicator dyes. Cell Calcium 27 (2), 97–106.
Gutsmann, T., Heimburg, T., Keyser, U., Mahendran, K.R., Winterhalter, M., 2015. Protein reconstitution into freestanding planar lipid membranes for electrophysiological characterization. Nat. Protoc. 10 (1), 188–198.
Heitz, B.A., Xu, J., Hall Jr., H.K., Aspinwall, C.A., Saavedra, S.S., 2009. Enhanced long-term stability for single ion channel recordings using suspended poly (lipid) bilayers. J. Am. Chem. Soc. 131 (19), 6662–6663.
Hirano-Iwata, A., Aoto, K., Oshima, A., Taira, T., Yamaguchi, R.T., Kimura, Y., Niwano, M., 2010. Free-standing lipid bilayers in silicon chips-membrane stabilization based on microfabricated apertures with a nanometer-scale smoothness. Langmuir 26 (3), 1949–1952.
Hirano-Iwata, A., Ishinari, Y., Yoshida, M., Araki, S., Tadaki, D., Miyata, R., Ishibashi, K.,

Yamamoto, H., Kimura, Y., Niwano, M., 2016. Reconstitution of human ion channels into solvent-free lipid bilayers enhanced by centrifugal forces. Biophys. J. 110 (10), 2207–2215.
Ishmukhametov, R.R., Russell, A.N., Berry, R.M., 2016. A modular platform for one-step assembly of multi-component membrane systems by fusion of charged proteoliposomes. Nat. Commun. 7, 13025.
Jezierski, T., Adamkiewicz, E., Walczak, M., Sobczynska, M., Gorecka-Bruzda, A., Ensminger, J., Papet, E., 2014. Efficacy of drug detection by fully-trained police dogs varies by breed, training level, type of drug and search environment. Forensic Sci. Int. 237, 112–118.
Kalsi, S., Powl, A.M., Wallace, B.A., Morgan, H., de Planque, M.R., 2014. Shaped apertures in photoresist films enhance the lifetime and mechanical stability of suspended lipid bilayers. Biophys. J. 106 (8), 1650–1659.
Kang, D.H., Han, W.B., Choi, N., Kim, Y.J., Kim, T.S., 2018. Tightly sealed 3D lipid structure monolithically generated on transparent SU-8 microwell Arrays for biosensor applications. ACS Appl. Mater. Interfaces 10 (47), 40401–40410.
Kanjirakat, A., Sadr, R., 2016. Near-wall velocity profile measurement for nanofluids. AIP Adv. 6 (1), 015308.
Korman, C.E., Megens, M., Ajo-Franklin, C.M., Horsley, D.A., 2013. Nanopore-spanning lipid bilayers on silicon nitride membranes that seal and selectively transport ions. Langmuir 29 (14), 4421–4425.
Kozlov, M.M., Chernomordik, L.V., 2015. Membrane tension and membrane fusion. Curr. Opin. Struct. Biol. 33, 61–67.
Lazarowski, L., Dorman, D.C., 2014. Explosives detection by military working dogs: olfactory generalization from components to mixtures. Appl. Anim. Behav. Sci. 151, 84–93.
Lei, G., MacDonald, R.C., 2003. Lipid bilayer vesicle fusion: intermediates captured by high-speed microfluorescence spectroscopy. Biophys. J. 85 (3), 1585–1599.
Lin, C.M., Li, C.S., Sheng, Y.J., Wu, D.T., Tsao, H.K., 2012. Size-dependent properties of small unilamellar vesicles formed by model lipids. Langmuir 28 (1), 689–700.
Lynden-Bell, R.M., Rasaiah, J.C., 1996. Mobility and solvation of ions in channels. J. Chem. Phys. 105 (20), 9266–9280.
Maricq, A.V., Peterson, A.S., Brake, A.J., Myers, R.M., Julius, D., 1991. Primary structure and functional expression of the 5HT3 receptor, a serotonin-gated ion channel. Science 254 (5030), 432–437.
Minami, H., Sugawara, M., Odashima, K., Umezawa, Y., Uto, M., Michaelis, E.K., Kuwana, T., 1991. Ion channel sensors for glutamic acid. Anal. Chem. 63 (23), 2787–2795.
Misawa, N., Osaki, T., Takeuchi, S., 2018. Membrane protein-based biosensors. J. R. Soc. Interface 15 (141), 1–17.
Na, J.H., Shin, J., Jung, Y., Lim, D., Shin, Y.K., Yu, Y.G., 2013. Bacterially expressed human serotonin receptor 3A is functionally reconstituted in proteoliposomes. Protein Expr. Purif. 88 (2), 190–195.
Nordlund, G., Brzezinski, P., von Ballmoos, C., 2014. SNARE-fusion mediated insertion of membrane proteins into native and artificial membranes. Nat. Commun. 5, 4303.
Oshima, A., Hirano-Iwata, A., Mozumi, H., Ishinari, Y., Kimura, Y., Niwano, M., 2013. Reconstitution of human ether-a-go-go-related gene channels in microfabricated silicon chips. Anal. Chem. 85 (9), 4363–4369.
Ota, S., Suzuki, H., Takeuchi, S., 2011. Microfluidic lipid membrane formation on microchamber arrays. Lab Chip 11 (15), 2485–2487.
Pantazatos, D.P., Pantazatos, S.P., MacDonald, R.C., 2003. Bilayer mixing, fusion, and lysis following the interaction of populations of cationic and anionic phospholipid bilayer vesicles. J. Membr. Biol. 194 (2), 129–139.
Rideau, E., Dimova, R., Schwille, P., Wurm, F.R., Landfester, K., 2018. Liposomes and polymersomes: a comparative review towards cell mimicking. Chem. Soc. Rev. 47 (23), 8572–8610.
Rodriguez, N., Pincet, F., Cribier, S., 2005. Giant vesicles formed by gentle hydration and electroformation: a comparison by fluorescence microscopy. Colloids Surfaces B Biointerfaces 42 (2), 125–130.
Römer, W., Steinem, C., 2004. Impedance analysis and single-channel recordings on nano-black lipid membranes based on porous alumina. Biophys. J. 86 (2), 955–965.
Sato, K., Pellegrino, M., Nakagawa, T., Nakagawa, T., Vosshall, L.B., Touhara, K., 2008. Insect olfactory receptors are heteromeric ligand-gated ion channels. Nature 452 (7190), 1002–1006.
Schindler, H., Rosenbusch, J.P., 1978. Matrix protein from Escherichia coli outer membranes forms voltage-controlled channels in lipid bilayers. Proc. Natl. Acad. Sci. Unit. States Am. 75 (8), 3751–3755.
Stamou, D., Duschl, C., Delamarche, E., Vogel, H., 2003. Self-assembled microarrays of attoliter molecular vessels. Angew. Chem. 42 (45), 5580–5583.
Stebelska, K., Dubielecka, P.M., Sikorski, A.F., 2005. The effect of PS content on the ability of natural membranes to fuse with positively charged liposomes and lipoplexes. J. Membr. Biol. 206 (3), 203–214.
Studer, A., Demarche, S., Langenegger, D., Tiefenauer, L., 2011. Integration and recording of a reconstituted voltage-gated sodium channel in planar lipid bilayers. Biosens. Bioelectron. 26 (5), 1924–1928.
Sumitomo, K., McAllister, A., Tamba, Y., Kashimura, Y., Tanaka, A., Shinozaki, Y., Torimitsu, K., 2012. Ca2+ ion transport through channels formed by alpha-hemolysin analyzed using a microwell array on a Si substrate. Biosens. Bioelectron. 31 (1), 445–450.
Syeda, R., Holden, M.A., Hwang, W.L., Bayley, H., 2008. Screening blockers against a potassium channel with a droplet interface bilayer array. J. Am. Chem. Soc. 130 (46), 15543–15548.
Thompson, A.J., R Lummis, S., 2006. 5-HT3 receptors. Curr. Pharmaceut. Des. 12 (28), 3615–3630.
Tiefenauer, L., Demarche, S., 2012. Challenges in the development of functional assays of membrane proteins. Materials 5 (12), 2205–2242.
Turner, A.P.F., 1997. Switching channels makes sense. Nature 387, 555.
Urban, M., Kleefen, A., Mukherjee, N., Seelheim, P., Windschiegl, B., Vor der Bruggen, M., Kocer, A., Tampe, R., 2014. Highly parallel transport recordings on a membrane-on-nanopore chip at single molecule resolution. Nano Lett. 14 (3), 1674–1680.
Uto, M., Michaelis, E.K., Hu, F., Umezawa, Y., Kuwana, T., 1990. Biosensor development with a glutamate receptor ion-channel reconstituted in a lipid bilayer. Anal. Sci. 6 (2), 221–225.
Watanabe, R., Soga, N., Fujita, D., Tabata, K.V., Yamauchi, L., Hyeon Kim, S., Asanuma, D., Kamiya, M., Urano, Y., Suga, H., Noji, H., 2014. Arrayed lipid bilayer chambers allow single-molecule analysis of membrane transporter activity. Nat. Commun. 5, 4519.
Watanabe, R., Soga, N., Hara, M., Noji, H., 2016. Arrayed water-in-oil droplet bilayers for membrane transport analysis. Lab Chip 16 (16), 3043–3048.
Yang, J., 1990. Ion permeation through 5-hydroxytryptamine-gated channels in neuroblastoma N18 cells. J. Gen. Physiol. 96 (6), 1177–1198.